

Generation of SST anomalies in the midlatitudes

Dietmar Dommenget and Mojib Latif

Max Planck Institut für Meteorologie

Bundesstr. 55, D-20146 Hamburg

email: dommenget@dkrz.de

submitted to J. Climate

ISSN 0937-1060

January 10, 2000

Contents

1	Introduction	4
2	Model description	5
2.1	The Ocean Mixed Layer Models	6
2.1.1	<i>MIX</i> ₅₀	7
2.1.2	<i>MIX</i> _{season}	8
2.1.3	<i>MIX</i> _{dynamic}	8
3	Model comparison	10
3.1	The standard deviation of the SST anomalies	11
3.2	The redness of the SST anomalies	13
3.3	The seasonally varying persistence of SST anomalies	15
3.4	The spectral distribution of the SST anomalies	16
3.4.1	The test criteria	16
3.4.2	Model time series	17
3.4.3	Observational time series	17
3.4.4	Results of the spectral hypothesis test	18
4	Sensitivity of the SST variability in midlatitudes to different physical processes	20
4.1	Wind amplified mixing of the ocean	22
4.2	Entrainment of sub-mixed layer water	23
4.3	Variability of the mixed layer depth	25
4.4	Damping by ocean heat flux	25
4.5	Re-emergence of temperature anomalies	26
5	Summary and discussion	27

Abstract

Analyses of monthly mean sea surface temperatures (SST) from a hierarchy of global coupled ocean-atmosphere models have been carried out with the focus on the midlatitudes (20N-45N). The spectra of the simulated SSTs have been tested against the null hypothesis of Hasselmann's stochastic climate model, which assumes an AR(1)-process for the SST variability. It has been found that the spectra of the SST variability in CGCMs with fully dynamical ocean models are significantly different from the AR(1)-process, while the SST variability in an AGCM coupled to a slab ocean is consistent with an AR(1)-process. The deviation of the SST variability in CGCMs with fully dynamical ocean models from the AR(1)-process are not characterized by spectral peaks but are due to a different shape of the spectra. This can be attributed to local air-sea interactions which can be simulated with an AGCM coupled to a slab ocean with dynamical varying mixed layer depth.

1 Introduction

Understanding the causes of natural climate variability is one of the main goals of climate research, whereby the interaction between the atmosphere and the ocean is one of the main causes of natural climate variability on the time scale from seasons to decades. The stochastic climate model introduced by Hasselmann (1976) attempts to explain the mechanism of natural climate variability by dividing the climate system into a fast system and a slow system. In this model the atmosphere is the fast system which is represented by white noise. The variability of the ocean, which is regarded as the slow component of the climate system, is explained by the integration of the atmospheric noise. In this picture the ocean is merely a passive part of the climate system, which amplifies the long-term variability, due to its large heat capacity, but dynamical processes in the ocean are not considered.

The resulting stochastic model of the SST variability is described by an autoregressive process of the first order (AR(1)-process), which is the simplest statistical model that can be applied to a stationary process. The stochastic climate model introduced by Hasselmann is therefore often chosen as the null hypothesis of SST variability.

Frankignoul and Hasselmann (1977) have shown that the observed interannual SST variability in the midlatitudes is consistent with this null hypothesis. In a more recent work Hall and Manabe (1997) have shown that the SST variability at some locations in the midlatitudes cannot be adequately explained by an AR(1)-process. They argue that the SST variability in these locations is influenced by meso-scale eddies. However, a comprehensive overview on the interannual SST variability in the midlatitudes is given in Frankignoul (1985).

On the decadal time scales, the characteristics of the observed SST variability are still unclear due to the limited lengths of the observed SST records. However, in a recent work Sutton and Allen (1997) have found some indication that the SST variability in the northern Atlantic may be predictable on the decadal time scales, due to the advection of temperature anomalies within the Gulf stream extension.

Due to the limited lengths of observed SST records it may be instructive to study additionally the decadal SST variability in coupled global circulation models (CGCMs). In these simulations many different ocean-atmosphere coupled modes have been found, which yields increased SST variability on the decadal time scales (e.g., Latif and Barnett (1994); Manabe and Stouffer (1996); Gu and Philander (1997)). A comprehensive overview of the decadal variability simulated in coupled models can be found in Latif (1997).

Here we have a closer look at the null hypothesis for the question of midlatitude SST variability, by comparing models with different ocean models. We test whether the large-scale features of the observed SST variability can be simulated by a simple global slab ocean-atmosphere coupled model, which can be regarded as a numerical realization of the null hypothesis (AR(1)-process) of Hasselmann's stochastic climate model. We shall address this question by comparing the results obtained from the simple slab ocean model, with the

observations and with a hierarchy of different ocean models coupled to the same atmosphere model. By doing so, we hope to identify some internal processes in the ocean which are important for the SST variability on seasonal to decadal time scales.

The paper is organized as follows. In the first section we introduce the different model simulations used in this study. In section 2 we carry out a comparison of the SST variability in the different models and in the observations. The results of the model comparison leads us to the discussion of the sensitivity of the SST variability to different physical processes in section 3. We concluded our paper with a summary and a discussion of our results.

2 Model description

A list of the simulations can be found in the table [1]. The ECHAM Atmospheric Model has been used in all simulations. ECHAM is a complete atmosphere general circulation model described by Roeckner et al. (1992). ECHAM has been used in two different versions (ECHAM3 and ECHAM4) and in two different resolutions (T21, T42). In the following, the differences in the atmosphere model will not be discussed and we consider the differences in the ECHAM versions not relevant for this analysis.

coupled model	number of years	spatial resolution	short description of Ocean Model
ECHAM4 - HOPE2	118	2.8125° x 2.8125°*)	fully dynamical, z-levels
ECHAM4 - OPYC	240	2.8125° x 2.8125°*)	fully dynamical, isopycnal, variable mixed layer parameterization
ECHAM3 - LSG	700	5.625° x 5.625°	fully dynamical, z-levels
ECHAM3 - MIX ₅₀	500	5.625° x 5.625°	slab ocean, 50meter fixed mixed layer
ECHAM3 - MIX _{season}	300	5.625° x 5.625°	slab ocean, seasonal mixed layer
ECHAM3 - MIX _{dynamic}	300	5.625° x 5.625°	slab ocean, dynamical mixed layer
*)The ocean model has a meridional resolution of 0.5° within the region 10°N - 10°S			

Table 1: List of simulations used in this study.

The main differences in the simulations are due to the different ocean models. Therefore, the simulations can be divided into two groups. In the first group we have three coupled

models with fully dynamical ocean models and in the second group we have coupled model simulations with slab ocean models. The fully dynamical ocean models try to simulate all physical processes in the ocean. The different models, however, employ different approaches to reach this goal.

In the HOPE and the LSG models, the ocean quantities are organized on z-levels, whereby the spatial and temporal resolutions of the HOPE model are significantly higher. The LSG model has a fixed mixed layer parameterization which is simply realized by an increased mixing in the surface layer, which has a depth of 50 meters, and by integrating the surface layer with a shorter time step of one day compared to the time step of lower levels of one month. In the HOPE model the mixed layer parameterization is kept more variable by introducing additional mixing at all levels for which the temperature differs from the temperature of the surface level by a prescribed threshold.

The OPYC model has a completely different structure. Here, the physical quantities are calculated on isopycnal levels. The OPYC model also includes a dynamical mixed layer model, which determines the depth and the temperature of the mixed layer. Therefore, the OPYC model is the only fully dynamical model in which the mixed layer depth is a dynamical quantity.

All three simulations exhibit El Niño-like behavior in the tropical Pacific. The El Niño-like variability simulated by the HOPE and OPYC models is much stronger than that in the ECHAM3-LSG model. However, the ECHAM3-LSG simulation has the advantage that the setup of the simulation is identical to the setup of the slab ocean simulations, whereby only the ocean model has been exchanged. For more detailed descriptions of the CGCMs the reader is referred to the following publications: For the ECHAM3-LSG CGCM see Maier-Reimer et al. (1993), Roeckner et al. (1992) and Voss (1998). The ECHAM4-HOPE2 CGCM is described in Frey et al. (1997). For the ECHAM4-OPYC CGCM experiment see Bacher et al. (1998) and Roeckner et al. (1996).

The general disadvantage of the fully dynamical ocean models is that it is difficult to determine which processes of the ocean models are relevant for certain structures of the variability. It is therefore necessary to compare the fully dynamical ocean models with ocean models that include fewer processes. From the differences between the fully dynamical ocean models and the simpler ocean models, one can determine the relevant processes for certain characteristics of the variability. Therefore, we have conducted three experiments with so called ‘slab’ ocean models. The three different slab ocean models will be described in the following section.

2.1 The Ocean Mixed Layer Models

The basic idea of a slab ocean model is that the grid points of the ocean model are not interacting with each other, and that the SST variability for each point of the ocean is forced

by the local interaction with the atmosphere. Such a model is a zero or one dimensional model, because it resolves only the vertical direction. Horizontal ocean dynamics such as advection by currents and waves are not simulated. The mean state of the ocean, which is strongly dependant on ocean currents, can therefore not be simulated correctly and must be introduced as a given climatology. However, a zero or one dimensional model is a good model to investigate different characteristics of a complex system, because the interactions in the model are kept very simple and different physical concepts can easily be introduced.

The null hypothesis of SST variability in the midlatitudes, described by Hasselmann's stochastic climate model (1976), assumes that the SST variability is well described by the integration of the atmospheric heat flux with the heat capacity of the ocean's mixed layer. All three slab ocean models simulate the SST variability by integrating the atmospheric heat flux with the heat capacity of the mixed layer, while the MIX_{50} slab ocean model exactly simulates the null hypothesis. For the MIX_{season} and $MIX_{dynamic}$ models we have considered a few characteristics, which may be relevant for the SST variability in the midlatitudes but are not considered by the MIX_{50} model.

2.1.1 MIX_{50}

The MIX_{50} slab ocean model is the simplest of the three slab ocean models used in this study. The complete ocean model is described by equation [1] for ocean points without sea-ice. A simple sea-ice model is included in all slab ocean models, but we shall not discuss the regions with sea-ice extent. The equation [1] represents the realization of the Hasselmann stochastic climate model, in which the SST variability is only forced by the atmosphere.

$$\frac{d}{dT}SST = \frac{1}{(C_p\rho_w d_{mix})} * F + \Delta T_c \quad (1)$$

- C_p = specific heat of sea water
- ρ_w = density of seawater
- d_{mix} = depth of mixed layer
- F = net atmospheric heat flux
- ΔT_c = climatology temperature correction

The only free parameter in this equation is the mixed layer depth d_{mix} , which was chosen to be 50 meters for all points. This value is roughly the global mean value for the mixed layer depth as was determined from the observations by Levitus (1982).

2.1.2 MIX_{season}

The MIX_{season} model is exactly the same model as the MIX_{50} model, but a seasonally dependant mixed layer depth d_{mix} is used. In the midlatitudes the depth of the mixed layer has a pronounced seasonal cycle. A theoretical study by Lemke (1984) has shown that a seasonal heat capacity of the ocean alters the spectra of an AR(1)-process. However, according to equation [1] a change in the mixed layer depth must have an effect on the SST variability. For the MIX_{season} model we therefore chose the mixed layer depth d_{mix} with a seasonal cycle. The seasonal cycle of d_{mix} has been determined by using the 50 years mean values of the mixed layer depth of the $MIX_{dynamic}$ model. The mean mixed layer depth d_{mix} over all ocean points between $20^{\circ}N$ and $60^{\circ}N$ averaged over the whole year is 52 meters, for the summer month is 26 meters and for the winter months is 99 meters.

2.1.3 $MIX_{dynamic}$

The midlatitudes exhibit some characteristics that may influence the SST variability which are not captured by the null hypothesis or the MIX_{50} slab ocean model. To further investigate the large-scale structures of the SST variability in midlatitudes, we assume that the MIX_{50} ocean model can be improved in such a way that the model produces the main characteristic of the SST variability. These characteristics of the midlatitudes are:

1. The mixed layer interacts with the sub-mixed layer ocean, which in general has a much colder temperature than the mixed layer. This temperature difference may damp the SST variability.
2. The depth of the mixed layer has a pronounced seasonal cycle and the depth of the mixed layer is a dynamical quantity which is determined by the state of the ocean and by the atmospheric forcing. A theoretical study by Lemke (1984) has shown that a seasonally varying heat capacity of the ocean alters the spectra of an AR(1)-process.
3. The mixed layer of the ocean is sensitive to wind stress. On stormy days, the ocean does not just integrate the atmospheric heat fluxes as on calm days, but it also entrains sub-mixed layer water into the mixed layer.

We consider that these characteristics of the local ocean-atmosphere interaction in the midlatitudes can be included within the framework of a slab ocean model. In addition to the MIX_{50} and MIX_{season} models, we now have to introduce a new equation to determine the mixed layer depth d_{mix} at each time step. Karraca and Mueller (1991) have used a Kraus and Truner type model (1967) to determine d_{mix} at different locations of the northern oceans by using the observed atmospheric fluxes and wind stresses. We implemented this model into our $MIX_{dynamic}$ ocean model to determine the SST and d_{mix} .

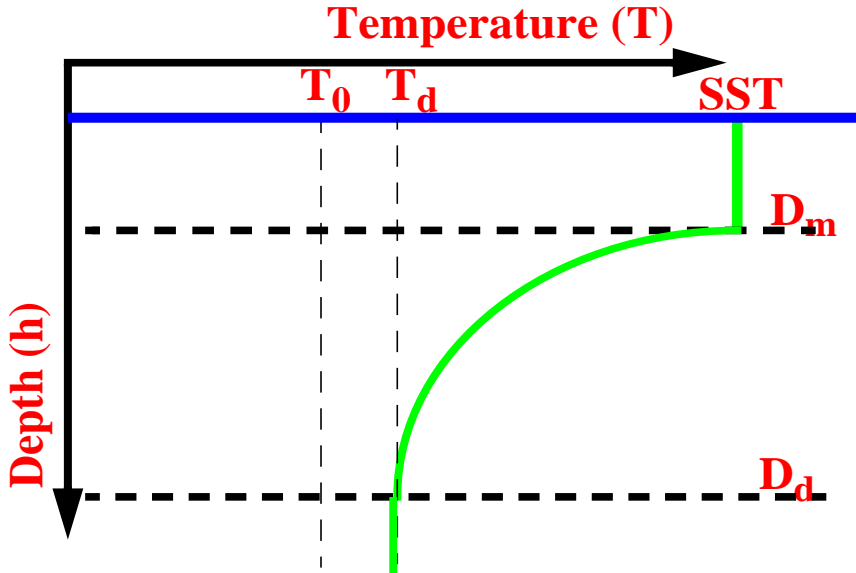


Figure 1: Schematic diagram illustrating the $MIX_{dynamic}$ mixed layer model.

$$R_0 = \int_0^{D_d} (T(h) - T_0) dh =: T_m H_q \quad (2)$$

$$R_1 = \int_0^{D_d} h(T(h) - T_0) dh =: R_0 H_p \quad (3)$$

$$F_q = \dot{R}_0 = \frac{1}{(C_p \rho_w)} F \quad (4)$$

$$F_p = \dot{R}_1 = C_1 C_{wind} \vec{\tau}^3 + C_2 H_p F_q \quad (5)$$

Figure 1 illustrates schematically the principle of the Kraus and Turner type ocean mixed layer model and introduces the new parameters. The integral R_0 in equation [2] determines the effective heat capacity of the ocean, while the integral R_1 in equation [3] determines the potential mechanical energy of the ocean due to the density distribution of the upper ocean. In contrast to equation [1], we now consider the heat capacity of the shaded area, which includes the mixed layer and, additionally, part of the thermocline of the upper ocean. Based on the two integrals R_0 and R_1 , the state of the ocean can be determined for each time step. The atmospheric mechanical energy input F_p and the atmospheric buoyancy flux will lead to a change in the two integrals R_0 and R_1 , as it is described by the equations [4] and [5]. In the original Kraus and Turner type ocean mixed layer the atmospheric buoyancy

flux is calculated by salinity and temperature changes. However, in our model we shall only consider the influence of the temperature changes, which reduces the atmospheric buoyancy flux to the atmospheric heat flux and also simplifies the integrals R_0 and R_1 to the expressions given in equation [2] and [3].

$$\frac{d}{dT}SST = \frac{F_q(d_{mix} + H_p) - F_p}{d_{mix}H_q} + \frac{F_{ocean}}{(C_p\rho_w d_{mix})} + \Delta T_c \quad (6)$$

$$F_{ocean} = C_{vo} * (T_c - SST) \quad (7)$$

$$\frac{d}{dT}d_{mix} = \frac{F_p - H_q F_q}{d_{mix}(SST - T_0 - \frac{SST - T_d}{\Theta})} + \Delta D_c \quad (8)$$

$$\Theta = \frac{SST - T_d}{T_d - T_0} \quad (9)$$

- F_q = *surface buoyancy flux*
- F_p = *mechanical energy input*
- H_q = *effective mixed layer depth*
- H_p = *reduced center of gravity*
- ΔT_c = *climatology temperature correction*
- ΔD_c = *climatology mixed layer depth correction*
- C_{vo} = *coupling parameter for the vertical heat exchange between the mixed layer and the sub-mixed layer ocean*
- T_c = *constant reference temperature*

The equations [6] and [8] determine the changes in the SST and in the mixed layer depth d_{mix} , respectively.

3 Model comparison

The comparison of the different simulations with each other and with the observations will focus on the null hypothesis. The comparison should show whether the large-scale features of the SST variability can be explained by the null hypothesis or if other processes are important. The large-scale features of the SST variability are characterized by the following three quantities:

1. The standard deviation of SST anomalies,
2. The redness of SST anomalies

3. The spectral distribution of SST anomalies

The standard deviation of the SST anomalies is the most important characteristic for our comparison, since it is a relatively robust quantity and it is not significantly affected by the interpolation of the observations in space and time. The other two characteristics cannot be compared with the observations in all details because the calculation of the redness and the spectral distribution are affected by the interpolation and averaging of the SST data, as it is done to produce global observed SST fields.

3.1 The standard deviation of the SST anomalies

Figure 2 shows the standard deviations of the monthly mean SST anomalies for the different simulations and for the observed SST obtained from the GISST data set from 1903 to 1994 (Parker et al. 1995). Figure 3 shows the zonally averaged standard deviations for all the models and the observations, whereby only ocean points that do not frequently exhibit the coverage of sea ice have been taken into account.

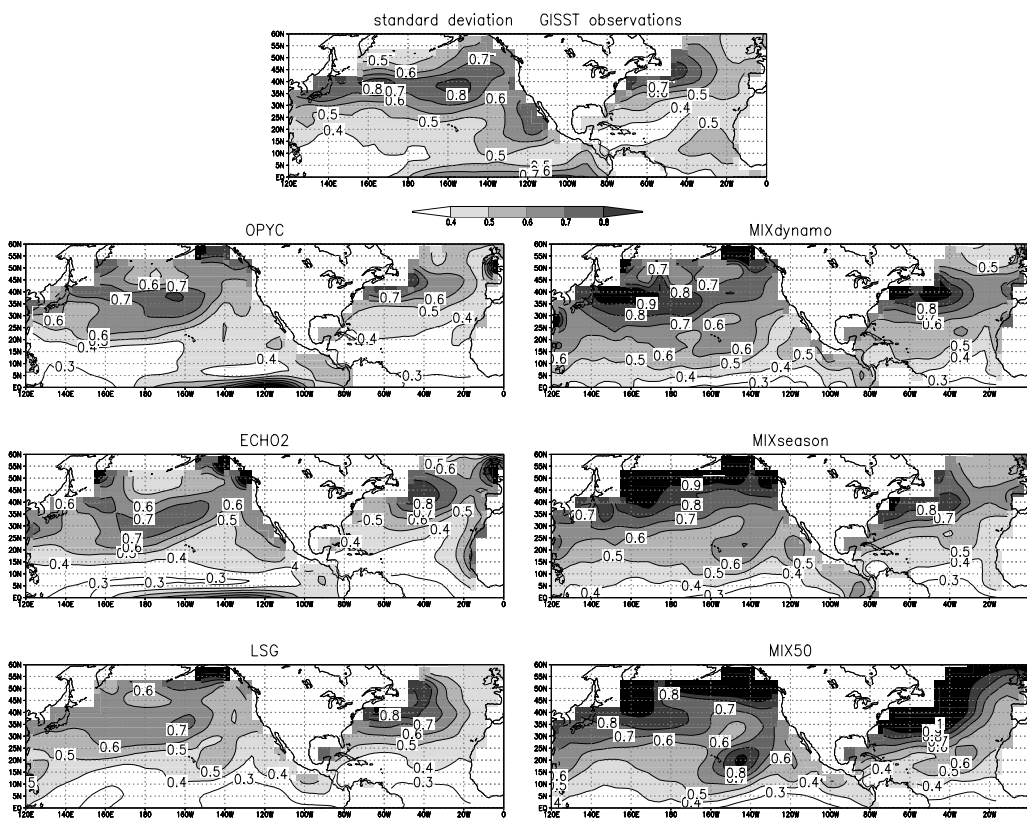


Figure 2: Standard deviations of the monthly mean SST anomalies for the different simulations and the observations.

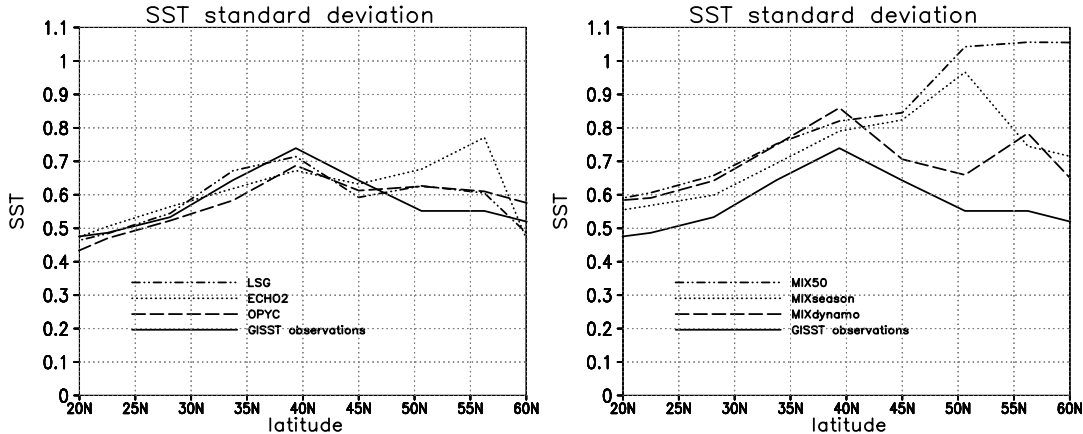


Figure 3: The zonally averaged standard deviation of the monthly mean SST anomalies of the fully dynamical ocean models (left) and of the slab oceans (right). The observations are shown for comparison.

The main spatial structure of the observed SST standard deviation is described by an increase of the variability from the lower latitudes up to about $40^\circ N$. The absolute maximum of variability is reached here and the standard deviation decreases towards higher latitudes. The maximum of the SST standard deviations in the Pacific as well as in the Atlantic seem to be tied to the regions of the storm tracks. The simulations with fully dynamical ocean models and the $MIX_{dynamic}$ simulation are very similar to the observations. Only the MIX_{50} and MIX_{season} simulations are quite different compared to the observations. Both do not exhibit an absolute maximum at $40^\circ N$, and both show a monotonic increase of the SST standard deviation with latitude. Overall, the variability of these two models is larger than in all other data sets, while the mismatch becomes largest poleward of $40^\circ N$.

3.2 The redness of the SST anomalies

The standard deviation of the SST anomalies do not alone describe the large-scale character of the SST variability. An important feature of the SST variability is the increase of the variance in the SST power spectra with period, which is the so called 'redness' of the spectra. If we consider that the spectra of the SST anomalies are basically following an AR(1)-process, than the redness can be estimated by the lag-1 correlation. The spectral density function $C(\omega)$ of an AR(1)-process is determined by:

$$C(\omega) = \frac{\sigma^2}{(1-a)^2 + \omega^2} \quad (10)$$

$C(\omega)$ = *spectral variance*

σ = *standard deviation*

ω = *frequency*

a = *lag-1 correlation based on monthly mean time series*

The increase of the spectral variance of an AR(1)-process with the period is only a function of the lag-1 correlation a in equation [10]. We therefore define our quantity for the 'redness' Q_{red} by equation [11].

$$Q_{red} = \frac{1}{(1-a)^2} \quad (11)$$

In Figure 4 the redness Q_{red} is shown for all models and the observations. In the comparison of the observations to the simulations, it becomes obvious that the redness of the observed SST variability is significantly smaller than in the simulations. In order to understand the differences in the redness of the spectra we have calculated the spectral distribution for all points of all data sets to determine the decadal SST and higher frequencies variances, which we will call "the low frequency variability" and "high-frequencies" variances, respectively. We defined the low-frequency variability as the spectral variance of the SST at about 20 years periods and the high frequency is defined by the spectral variance of the monthly periods. In Figure 5 the zonally averaged low-frequency variability, redness and high-frequency variance are shown.

The comparison of the different simulations with the observations shows, that the largest differences in the SST variance are at the high-frequency time-scale, while the differences in the low-frequency SST variance are much weaker. We therefore conclude that the smaller redness of the observed SST variability compared to the simulations is mainly due to the fact that the month to month variability in the observations is significantly larger than in all simulations. One possible reason for the significantly larger month to month variability in the observations is discussed below 3.4.3.

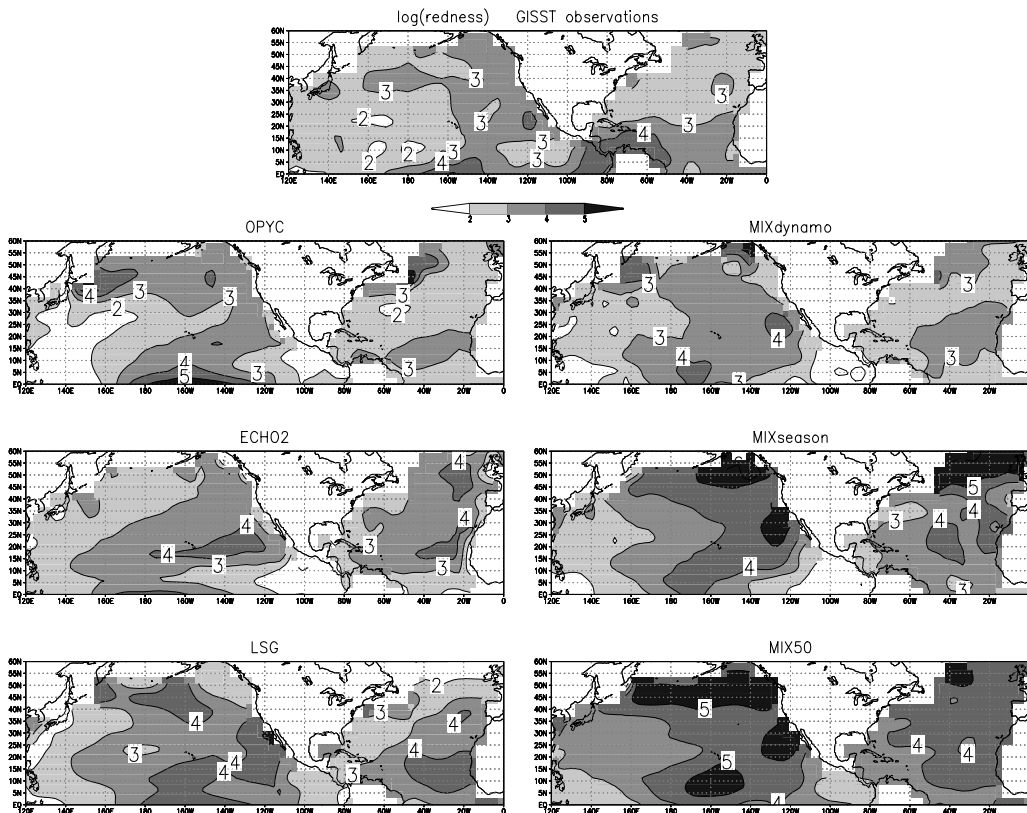


Figure 4: The ‘redness’ of the monthly mean SST anomalies for the different simulations and the observations.

We also found that the lag-1 correlation of the observed SST variability during 1903 - 1950 is significantly smaller than that during 1950 - 1994. We assume that this difference is a result of the lower density of SST measurements during this period. We therefore based our analyses of the lag-1 correlation of the observations on the time period 1950 - 1994. However, to calculate the spectral density at decadal time-scales we used the whole time range from 1903 - 1994. Although the larger monthly variability in the observations relative to all simulations is partly due to sampling problems, we discuss the differences between the simulations and the observations while keeping in mind these problems.

The redness simulated by the fully dynamical ocean models, the $MIX_{dynamic}$ model and that of the observations are of the same order. However, we have to keep in mind that the redness of the observed SST anomalies may be reduced by the sampling problems noted above. The rednesses of the MIX_{50} and MIX_{season} simulations are significantly larger than in the observations and all other simulations, whereby the larger rednesses of the MIX_{50} and MIX_{season} simulation can mainly be explained by the much SST variances on the high-frequency time-scale (Figure 5). The differences in the low-frequency or decadal range are, on the other hand, much smaller.

The more realistic redness of the $MIX_{dynamic}$ simulation compared to the MIX_{50} and

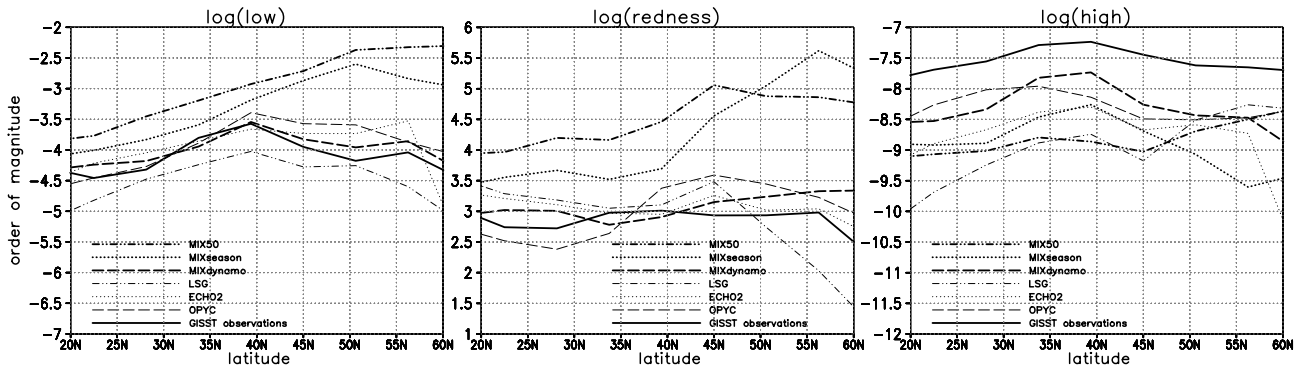


Figure 5: The left plot shows the zonally averaged low frequency (1/20yrs) variance of the SST anomalies and the right plots shows the high-frequency (1/2months) variance of the different models and the observations. The middle plot shows the zonally averaged ‘redness’ of the monthly mean SST anomalies.

MIX_{season} simulations is mainly due to the introduction of the ocean heat flux F_{ocean} in equation [6], which damps the SST variability.

3.3 The seasonally varying persistence of SST anomalies

In summer, the mixed layer depth in midlatitudes amounts to about 20 meters, while in winter the mixed layer is deeper than 150 meters. It has to be considered that the varying mixed layer depth will lead to different integrations of atmospheric heat flux in the different seasons. A larger mixed layer depth d_{mix} will lead to larger SST persistence. Therefore, the lag-1 correlations of the SST anomalies should be smaller in summer than in winter.

In the observations, the difference is mostly positive in the midlatitudes, which indicates that the SST anomalies are more persistent during winter (see Figure 6). The same general picture is found in the $MIX_{dynamic}$, MIX_{season} , HOPE and the OPYC simulations with an even stronger amplitude. The MIX_{50} and the LSG, however, exhibit the opposite behavior.

The $MIX_{dynamic}$, MIX_{season} , HOPE and the OPYC simulations have in common that the ocean model includes the seasonal cycle of the mixed layer depth, while the MIX_{50} and the LSG simulations do not. Thus seasonality of the mixed layer depth is an important process for the simulation of midlatitude SST variability.

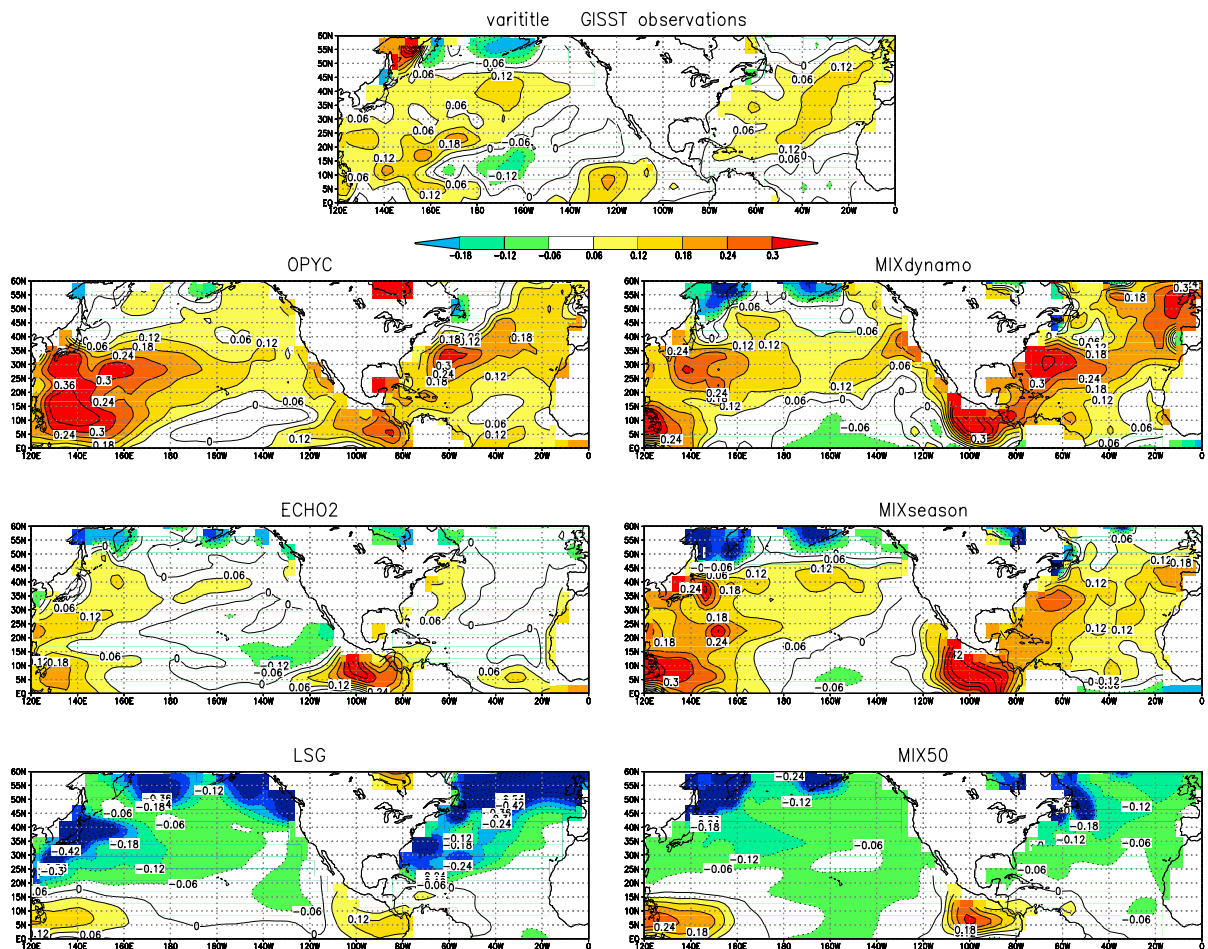


Figure 6: The differences between the lag-1 correlations between winter and summer for the different simulations and the observations. Positive values indicate larger lag-1 correlations in winter.

3.4 The spectral distribution of the SST anomalies

Hasselmann's simplest stochastic climate model yields a spectrum of the SST anomalies characteristic of an AR(1)-process.

3.4.1 The test criteria

For a statistical test of the SST variability against the null hypothesis (the AR(1) process) we shall assume that differences can best be shown by comparing the variance spectra of the SST time series and the fitted AR(1)-process. We therefore determine the spectral coefficients of the spectra s_i from the time series under consideration and those of the hypothesis spectrum t_i by equation [10]. We then define our test quantity T as:

$$T = \frac{1}{\log(10.0)\log(C_{conf})} * \sqrt{\sum_{i=2}^N \frac{(\log(s_i) - \log(t_i))^2}{N-1}} \quad (12)$$

T	=	<i>test value</i>
s_i	=	<i>spectral coefficient of spectra</i>
t_i	=	<i>spectral coefficient of hypothesis spectra</i>
N	=	<i>number of channels</i>
C_{conf}	=	<i>confidence level of hypothesis spectra (i.e. 95%)</i>

We assume that the spectral coefficients s_i are random fluctuations around the coefficients t_i of the hypothesis spectrum. The test quantity can therefore be interpreted as the integrated error of the spectrum relative to the hypothesis spectrum. In principle, the test quantity T is not dependent on the length of the time series, since T has been normalized by $\log(C_{conf})$. However, the time series has to be long enough to accurately determine the spectral coefficients. We test our results with Monte Carlo statistics obtained from 1000 realizations of AR(1)-processes.

3.4.2 Model time series

The output of the simulations is given by monthly mean values, while the time step is of the order of one day or even shorter. If we want to test the SST time series of the simulations against a statistical model like the AR(1)-process, we have to consider that the monthly mean values are the result of an averaging process which changes the spectral distribution of the SST variability.

In Figure 7, the spectrum of the MIX_{50} SST anomalies at $180^\circ, 35^\circ N$ is shown. In addition, two different spectral distributions have been calculated based on the standard deviation and lag-1 correlation. It can clearly be seen that the spectrum of the SST anomalies is following the fitted spectrum obtained from monthly means. For the low frequency and high frequency ranges the differences between the theoretical spectra are significantly larger than the statistical uncertainty. Thus, the effect of the averaging process has to be taken into account when the spectral hypothesis is tested. Instead of testing the spectrum of the monthly mean SST time series against a fitted AR(1)-process, we shall test the hypothesis that the monthly mean SST time series is a monthly mean averaged AR(1)-process, assuming that the original SST time series is an AR(1)-process.

3.4.3 Observational time series

We have shown that the averaging process, that has to be applied to produce the monthly means changes significantly the spectral distribution of the SST anomalies. Although, for the simulations, the process of producing the monthly means is the same for all time steps and grid points, it varies significantly in the observations. In the GISST data set, the SST value of a single month at a certain point is an average over an unknown number of measurements,

MIX-50

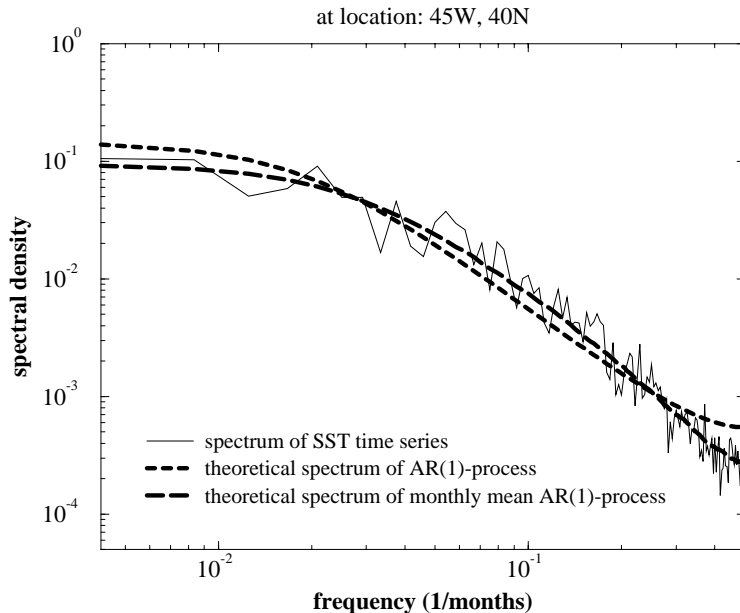


Figure 7: Spectrum of the SST anomalies simulated in the MIX_{50} simulation (at the location: $40^{\circ}N, 40^{\circ}W$) compared to two differently fitted spectral distributions. See text for details.

and the time intervals between the individual measurements are not known and are likely to be variable. This problem increases the uncertainty of the observational SST spectra and makes it difficult or impossible to compare the observed SST with simulated SST spectra. Therefore, a statistical test as proposed in section 3.4.1 can not be applied to the observation or at least the test value T must be significantly increased.

3.4.4 Results of the spectral hypothesis test

Based on the Monte Carlo distribution of the test value T , we can define confidence levels for the hypothesis that our SST spectra are not in statistical agreement with a monthly mean averaged AR(1)-process, which are shown in Figure 8. The confidence level of the observations is only shown for the sake of completeness, while we have to keep in mind that the test is problematic as discussed in section 3.4.3.

The confidence levels of the MIX_{50} and the MIX_{season} simulations are mostly less than 65%, which indicates that the SST variabilities are basically consistent with an AR(1)-process. This supports the idea behind Hasselmann's stochastic climate model and is in clear contrast to the simulations with the fully dynamical ocean models, which all have much higher confidence levels ($> 95\%$). This indicates that the ocean dynamics, which are only included in the fully dynamical ocean models, clearly alter the spectra of the SST anomalies to a spectral distribution that is not consistent with an AR(1)-process.

The difference between the AR(1)-process and the spectra of the SST anomalies in the fully dynamical simulations is characterized by a slower but longer increase of the SST variance from shorter to longer periods, which leads to increased variance of the SST on the

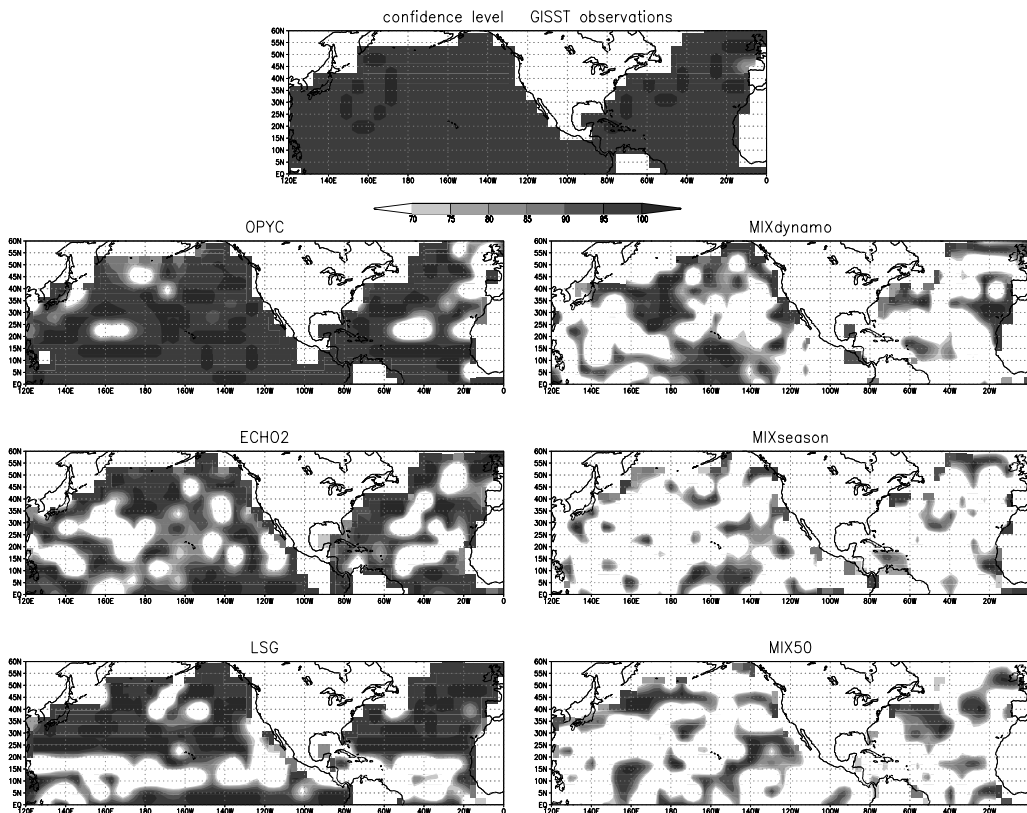


Figure 8: The confidence levels for rejecting the null hypothesis of an $AR(1)$ -process based on a Monte Carlo distribution of the test value T for the different simulations and the observations.

seasonal and the decadal time-scales relative to the fitted $AR(1)$ -process (see Figure 9).

The spectra of the $MIX_{dynamic}$ simulations are also significantly different to the fitted $AR(1)$ -process, but the basic structure of the spectra is significantly different from those obtained from the fully dynamical ocean models. The most striking feature of the SST spectrum of the $MIX_{dynamic}$ simulation compared to the observations and the fully dynamical simulations is the missing increase of the SST variance from the interannual time-scale to the decadal time-scale. Thus the influences of the sub-mixed layer ocean to the SST variability on decadal time scales can not be simulated by a purely damping sub-mixed layer ocean.

The results of this comparison indicate that the source of decadal time-scale SST variability in midlatitudes is not just the 'redness' of the spectra due to the integration of atmospheric forcing as found in the MIX_{50} and MIX_{season} simulations. Moreover, the decadal time scale SST variability in the simulations with fully dynamical ocean models is caused by the interaction between the mixed layer and the sub-mixed layer ocean.

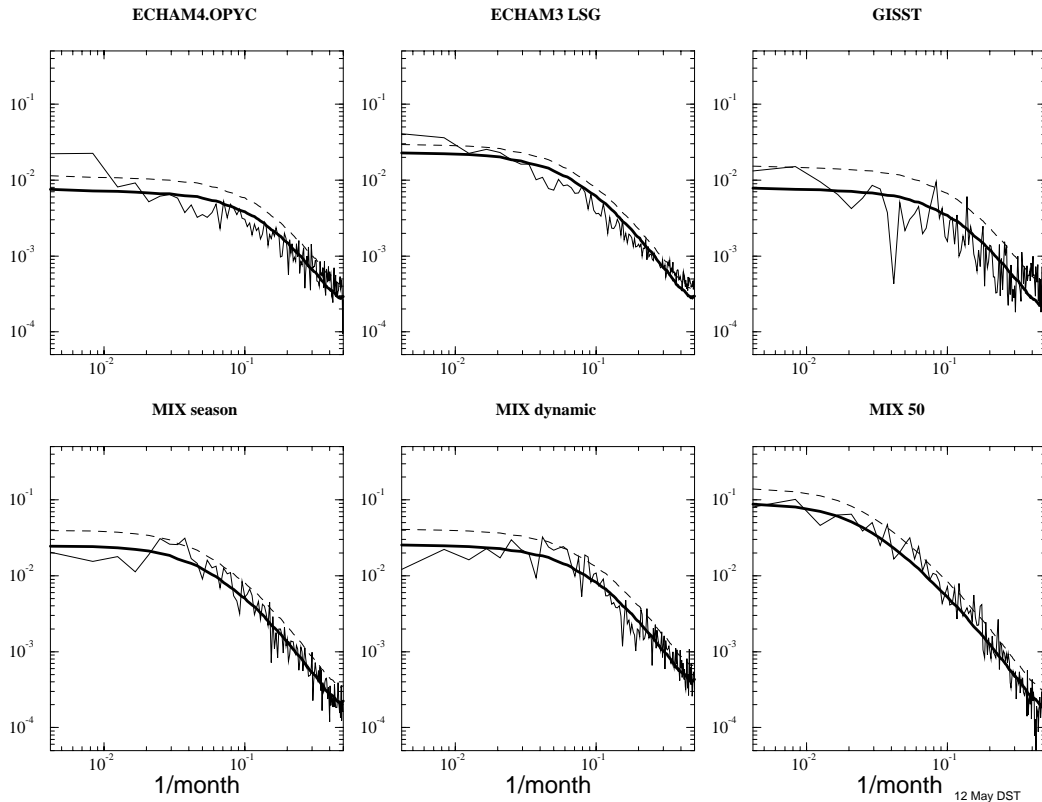


Figure 9: Spectra of the SST anomalies (at the location: $35^{\circ}N$, $40^{\circ}W$) compared to the fitted spectra of a monthly averaged $AR(1)$ -process for the different simulations and the observations.

4 Sensitivity of the SST variability in midlatitudes to different physical processes

We now study the sensitivity of the SST variability in midlatitudes to different physical processes by comparing the $MIX_{dynamic}$ simulation with different sensitivity experiments, in which we have excluded some of the processes that are simulated in the full $MIX_{dynamic}$ simulation (Table 2). This comparison will show which processes are important for the large-scale characteristics of the SST variability in midlatitudes.

The atmospheric model used in all these simulations is the ECHAM3(T21) model. The different physical processes and the time scales on which they act are listed in Table 3.

experiment	number of years	short description of the slab ocean model
MIX_{50}	300	slab ocean, 50meter fixed mixed layer depth
MIX_{season}	300	slab ocean, with seasonal mixed layer depth
$MIX_{noentrain}$	10	slab ocean, using equation [1] for the SST and equation [8] for d_{mix}
MIX_{KT}	10	like $MIX_{dynamic}$ but setting $F_{ocean} = 0.0$ in equation [6]
$MIX_{dynamic}$	300	slab ocean, with dynamic ocean mixed layer

Table 2: List of slab ocean models used in this study.

physical process	time scale
Wind amplified mixing of the ocean	increased daily variability
Entrainment of sub-mixed layer water	increased monthly variability
Variability of the mixed layer depth	increased seasonal to interannual variability
Seasonal mixed layer depth	increased monthly variability in summer decreased monthly variability in winter
Damping by ocean heat flux	decreasing seasonal to decadal variability
Re-emergence of temperature anomalies	increasing interannual to decadal variability

Table 3: List of the physical processes that are included in the $MIX_{dynamic}$ simulation and are not included in the MIX_{50} simulation. In the right column, the time scale is listed on which the physical process is effecting the SST variability of the $MIX_{dynamic}$ simulation.

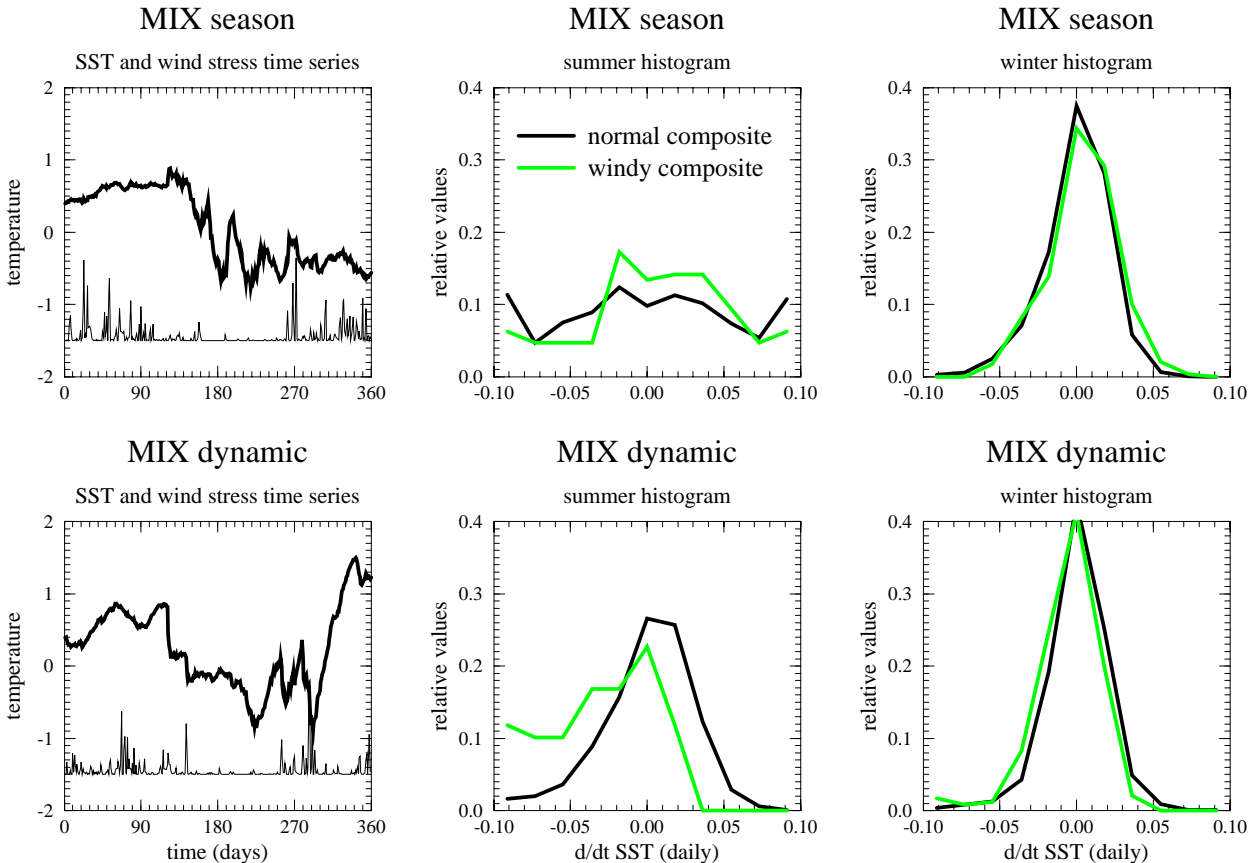


Figure 10: The left plots show a one year long time series of the SST anomalies (thick lines) and the wind stress $\vec{\tau}^2$ (thin lines) of the MIX_{season} and $MIX_{dynamic}$ simulations. The right and the middle plots show histograms of the daily $\frac{d}{dt}SST$. The windy composite histograms are for days with $\vec{\tau}^2 > 0.2$.

4.1 Wind amplified mixing of the ocean

In the dynamic mixed layer ocean model $MIX_{dynamic}$ the SST is calculated following equation [6]. In this equation, the change of SST is a function of the mechanical energy input F_p , which is a function of the wind stress $\vec{\tau}$. In contrast, the change of the SST is only a function of the atmospheric heat flux in the MIX_{50} model.

In equation [5], a strong wind stress $\vec{\tau}$ will increase the mechanical energy input F_p , which will lead to negative SST changes in equation [6]. A positive mechanical energy input F_p will increase the mixed layer depth and sub-mixed layer water is entrained. While the sub-mixed layer ocean in this model is always colder than the SST, the entrainment of sub-mixed layer water has to result in a cooling of the SST.

To analyze the effect of the wind stress on the SST variability we compared the daily SST time series in the $MIX_{dynamic}$ simulation with the MIX_{50} simulation. Both models are integrated with a time step of one day.

In the $MIX_{dynamic}$ simulation, the SST exhibits characteristic decreases at the beginning and end of the summer (days 100 - 240). These SST changes coincide with strong wind

stresses (see Figure 10) and do not appear in the MIX_{season} model.

In the $MIX_{dynamic}$ simulation, a comparison of the two summer histograms shows that the histogram of the windy composite is significantly shifted to negative SST tendencies, while the normal composite is basically normally distributed. The same shift can be seen in the winter histograms, but it is not as strongly as in the summer histograms.

In the MIX_{season} simulation, the windy and the normal composite histograms are neither significantly different in summer nor in winter. However, neither of the two summer histograms of the MIX_{season} simulation are normally distributed. We conclude that, in the $MIX_{dynamic}$ simulation the SST changes during summer are significantly influenced by strong wind stress. These will lead to strong cooling of the SST mainly during spring and fall. The cooling of the SST normally lasts only one or two time steps, which will lead to increased power of the SST spectrum at the shortest simulated time periods.

In the $MIX_{dynamic}$ simulation, the sub-mixed layer ocean is always colder than the SST. In the real world, the temperatures of the ocean underneath the mixed layer are often warmer than the SST during the winter period at some locations in the midlatitudes. At these locations, strong wind stresses will lead to warming during the winter period.

In the dynamical mixed layer model of the $MIX_{dynamic}$ simulation, it is assumed that the temperature of the sub-mixed layer ocean is always colder than the SST. The effect of warmer sub-mixed layer temperatures can be included in the $MIX_{dynamic}$ simulation by introducing salinity into the buoyancy equations. This has not been done in this simulation to keep the model as simple as possible in the first realization, but can easily be introduced.

The wind induced mixing is the main reason why the $MIX_{dynamic}$ simulation is able to reproduce the observed enhancement of the standard deviation of the SST anomalies in the region of the storm tracks (see Figure 2), and this may also be the reason why the MIX_{50} and MIX_{season} simulations fail to reproduce this feature of the SST variability in the midlatitudes.

4.2 Entrainment of sub-mixed layer water

In the $MIX_{dynamic}$ simulation, the deepening of the mixed layer depth leads to entrainment of sub-mixed layer water into the mixed layer. As shown in the preceding section, the entrainment occurs usually during short-lived strong wind stress events.

The effect that the entrainment of sub-mixed layer water into the mixed layer has on the SST variability can be quantified by comparing two different slab ocean simulations. Therefore, we have integrated the simulation MIX_{kt} and $MIX_{noentrain}$. The MIX_{kt} simulation is similar to the $MIX_{dynamic}$ simulation, but the ocean heat flux F_{ocean} has been set to zero. The experiment $MIX_{noentrain}$ is the same as the MIX_{kt} simulation in all aspects, but the equation [6] for the SST change has been replaced by the equation [1] of the MIX_{season} and MIX_{50} simulations. A change in the mixed layer depth d_{mix} due to surface buoyancy flux

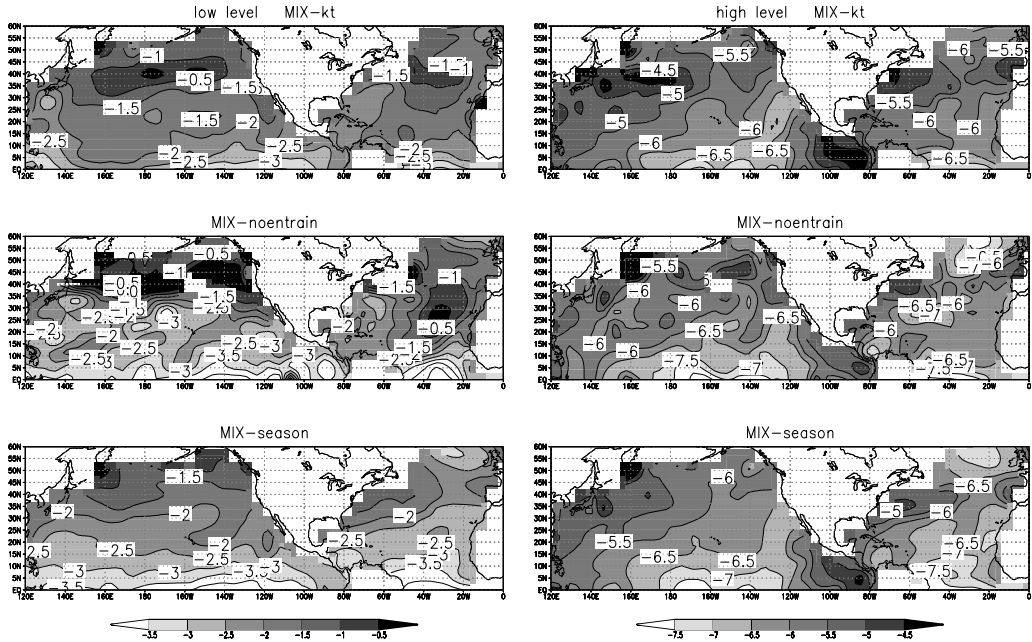


Figure 11: The plots show the low-frequency (left) and the high-frequency (right) variance of the SST anomalies of three different slab ocean simulations. The values are in relative orders of magnitudes. See text for details.

or mechanical energy input is still simulated in the $MIX_{noentrain}$ experiment, but it will not lead to a change in the SST due to entrainment of cooler sub-mixed layer water. We can therefore assume that the high frequency SST variability in the $MIX_{noentrain}$ simulation will be reduced relative to the MIX_{kt} simulation.

The Fourier spectra of the monthly mean SST anomalies for the different simulations have been calculated (Figure 11). On the left hand side, the average of the spectral coefficients from 24 month to 8 month periods is shown, which we shall refer to as the low frequency SST variability, and on the right hand side, the average of the spectral coefficients from $2\frac{2}{3}$ month to 2 month periods is shown, which we shall refer to as the high frequency SST variability.

The comparison of the low frequency variances indicates that the variance of the $MIX_{noentrain}$ simulation is significantly larger than in the MIX_{kt} simulation in the northern Pacific. However, we have to consider that the time series of the $MIX_{noentrain}$ simulation, which is only 10 years long, which may be too short to decide. However, it is possible that the entrainment of sub-mixed layer water can damp the SST variability in the Pacific north of $40^\circ N$, which may explain the smaller variance of the low frequency SST variance in the MIX_{kt} simulation.

The comparison of the high frequency variance in Figure 11 shows that the variance of the MIX_{kt} simulation is significantly larger than in the $MIX_{noentrain}$ simulation, especially

around $40^\circ N$. From this comparison, we can conclude that the entrainment of colder sub-mixed layer water into the mixed layer leads to increased SST variability on time-scales of weeks to months.

4.3 Variability of the mixed layer depth

The basic idea of slab ocean models is that the atmospheric heat flux is fully absorbed by the mixed layer. This is captured by the equations [1] and [6], in which the SST tendencies are proportional to the atmospheric heat fluxes F times the inverse of the heat capacity of the mixed layer, which, on the other hand, is proportional to the depth of the mixed layer d_{mix} .

While the entrainment of colder water from the sub-mixed layer ocean is leading to increased SST variability only on the shorter time scales, the correlation between the SST and the mixed layer depth due to the basic structure of equation [6] will lead to an increase of the SST variability over the entire frequency range.

This can be quantified by comparing the spectrum of the SST anomalies of the MIX_{kt} with the spectrum of the MIX_{season} and $MIX_{noentrain}$ simulations (Fig. 11). The MIX_{season} and $MIX_{noentrain}$ are identical simulations, with the only difference that the mixed layer depth d_{mix} is variable in the $MIX_{noentrain}$ simulation, while it is constant in the MIX_{season} simulation.

The low frequency variance of the SST in the $MIX_{noentrain}$ simulation is significantly larger than in the MIX_{season} simulation, while the high frequency variance is on similar levels in both simulations. This demonstrates that the variability of the mixed layer depth is increasing the interannual SST variability, while the entrainment of sub-mixed layer water into the mixed layer due to atmospheric wind stress variations is only effecting the short time scales of days to months.

4.4 Damping by ocean heat flux

An oceanic heat flux F_{ocean} , which is proportional to the SST anomalies has been introduced in the $MIX_{dynamic}$ simulation (see equation [6]). In Hasselmann's null hypothesis of midlatitude SST variability, it is assumed that the SST variability is only effected by the atmospheric heat fluxes and that, therefore, the mixed layer of the ocean is not exchanging heat with the sub-mixed layer ocean. In general, the temperature profile of the upper ocean in the midlatitudes shows a roughly exponential decrease of the temperature beneath the mixed layer (Fig. 1). The exponential decrease of the temperature indicates that the mixed layer and the sub-mixed layer ocean are exchanging heat. It is therefore important to consider an oceanic heat flux of the mixed layer to the sub-mixed layer ocean.

In the $MIX_{dynamic}$ simulation, the oceanic heat flux F_{ocean} is a pure damping, that is proportional to the strength of the SST anomalies, which therefore will be most effective

in the regions with the largest SST variability. In Figure 3, it can be seen that the SST variability of the MIX_{50} or MIX_{season} simulations is increasing with latitude and that the standard deviation in the mid and higher latitudes are significantly larger than those observed. The effect of the oceanic heat flux F_{ocean} in the $MIX_{dynamic}$ simulation is especially important in these regions, because it is damping the SST variability to more realistic values.

The strength of the oceanic heat flux parameter C_{vo} in equation [7] was chosen to be $4W/(m^2K)$, which is consistent with values found in literature for the vertical heat flux in the upper ocean. However, the SST anomalies in the midlatitudes of the $MIX_{dynamic}$ simulation are still too strong. A higher value for C_{vo} can reduce the SST variability in the $MIX_{dynamic}$ simulation further. A comparison of the $MIX_{dynamic}$ simulation with the MIX_{kt} simulation indicates that a value of $C_{vo} = 8.0W/(m^2K)$ would yield a more realistic SST variability in the $MIX_{dynamic}$ simulation.

The construction of the ocean heat flux F_{ocean} in the $MIX_{dynamic}$ simulation will not only effect the standard deviation of the SST variability, but it will also change the spectral distribution of the SST. Since F_{ocean} is proportional to the strength of the SST anomaly and the spectral variance is increasing with the period, the variability of longer time-scales will be damped more efficiently than short time variability. In Figure 9, the spectra of the SST variability of the $MIX_{dynamic}$ simulation is slightly decreasing from the interannual to the decadal time scale. In contrast to this behavior, the fully dynamical ocean model simulations show a significant increase of the SST variability from the interannual to the decadal time scale. This indicates that the formulation of the ocean heat flux F_{ocean} is missing important processes, which are producing the decadal time scale SST variability.

4.5 Re-emergence of temperature anomalies

In the construction of the slab ocean models we assumed that the mixed layer of the ocean is forced only by the atmosphere and that the ocean underneath the mixed layer is not effected by the atmosphere directly. The mixed layer of the ocean is exhibiting a distinct seasonal variation in the midlatitudes. The minimum of the mixed layer depth of about 20 meters is reached during summer and the maximum of about 200 meters during winter. In the early winter or late fall, the mixed layer is deepening from the summer to the winter depth and is thereby entraining the water of the layers underneath the summer mixed layer.

The temperature anomalies of the new winter mixed layer should, therefore, be stronger correlated with the temperature anomalies of the sub-mixed layer ocean than with the SST, which is supported by the findings of Namias and Born (1970, 1974). They found that SST anomalies in midlatitudes recur from one winter to the next, without being persistent during the summer. They speculated that the temperature signal is stored in the sub-mixed layer ocean during the summer month, when the mixed layer is shallow.

In the $MIX_{dynamic}$ simulation, the temperature of the ocean underneath the mixed layer

is parameterized by an exponential decrease from the SST to the constant deep ocean temperature T_d (see Figure 1). Therefore, temperature anomalies of the ocean underneath the mixed layer are only a function of the SST anomalies. The entrainment of sub-mixed layer water during the fall period in the $MIX_{dynamic}$ simulation does therefore not generate new SST anomalies due to the re-emergence of temperature anomalies from the sub-mixed layer ocean, it just damps the existing SST anomalies. This seems to be unrealistic assuming that the sub-mixed layer ocean is mainly independent of the actual atmospheric forcing and SST. In order to make the behavior of the temperature anomalies of the ocean underneath the mixed layer more realistic and to investigate the characteristics of the decadal time scale SST variability, which is not sufficiently strong in the $MIX_{dynamic}$ simulation, an improvement of the $MIX_{dynamic}$ simulation can be proposed.

In principle, the $MIX_{dynamic}$ simulation can be improved by keeping the temperature anomaly of the ocean underneath the mixed layer at the value which was present at the last time step before the spring jump occurs and conserving the temperature anomaly over the summer until the next fall, when the entrainment of the sub-mixed layer ocean increases the mixed layer depth again. During the entrainment of the sub-mixed layer water temperature anomalies re-emerge that have been formed during the last winter. This will lead to an increase of decadal time-scales SST variability. Alexander et al. (1996) have analyzed an one dimensional dynamical mixed layer ocean model, which includes the re-emergence of temperature anomalies, coupled to a stochastic atmosphere model. In their model simulation the spectrum of the SST anomalies is increasing from the interannual to the decadal time scales, which may be caused by the re-emergence of temperature anomalies as they conclude.

5 Summary and discussion

In this work, we compared different model simulations with the observations in order to test whether the large-scale SST variability in the midlatitudes of the Northern Hemisphere is consistent with the null hypothesis, presented by Hasselmann's stochastic climate model (1976). We conclude that the SST variability in the midlatitudes is significantly different from Hasselmann's simplest stochastic climate model and that the processes in the ocean which are responsible for this differences can be assigned.

Our conclusions are based on two basic findings: First, the comparison of the different simulations with the observations shows that the simulations with the fully dynamical ocean models and the observations are significantly different in terms of the large-scale features of the SST variability to the simple MIX_{50} or MIX_{season} simulations. Second, the statistical test of the spectral distribution of the SST variability in the different models revealed that only the simple MIX_{50} or MIX_{season} simulations can be regarded as AR(1)-processes, while in all other simulations the spectral distributions of the SST variability are significantly different from the spectral distributions of the AR(1)-processes.

In addition to the unrealistically enhanced SST variability in the MIX_{50} simulation, the redness of the SST, which describes the increase of the SST variance with increasing time periods, is also much larger in the MIX_{50} simulation than in the observations. Although the overall variance of the SST variability in the MIX_{50} simulation is larger than in the observations, the large redness of the SST variability in the MIX_{50} simulation leads to much weaker SST variability on the month to month time scale. In the realization of Hasselmann's stochastic climate model in the MIX_{50} simulation, the equation [1] for the integration of the atmospheric heat flux has only one free parameter, the mixed layer depth d_{mix} . Although the mixed layer depth of about 50 meters is a realistic assumption, one may argue that, for the stochastic climate model, a different mixed layer depth has to be chosen and the depth can be different at different locations of the ocean.

However, tuning of the mixed layer depth cannot modify the characteristics of the SST variability in the MIX_{50} simulation to be consistent with the observations. An increase of the mixed layer depth in order to decrease the standard deviation of the SST leads to further increase of the redness. A smaller mixed layer depth will increase the standard deviation of the SST, which is inconsistent with the observations.

We have also tested the spectral distribution of the SST variability against the hypothesis of an AR(1)-process. While we found that the MIX_{50} and the MIX_{season} simulations are basically consistent with an AR(1)-process, the spectral distribution of the SST variability in the simulations with fully dynamical ocean models and also, but to a lesser extent, in the $MIX_{dynamic}$ simulation are significantly different. The difference between the AR(1)-process and the SST spectra in the simulations with fully dynamical ocean models is characterized by a slower increase of the SST variance from the shorter time periods to the longer time periods, which leads to increased variance of the SST on the seasonal and the decadal time scale relative to the fitted AR(1)-process (see Figure 9).

The missing physical process causing the differences between the observed variability and that simulated by the simple MIX_{50} model are better represented in the dynamical slab ocean model $MIX_{dynamic}$. In this model, Hasselmann's stochastic climate model has been expanded by the introduction of a dynamical variation of the mixed layer depth. The following physical processes improve the spatial and temporal structures of the SST variability: Wind induced entrainment of sub-mixed layer water into the mixed layer, the seasonal cycle of the mixed layer depth and the heat exchange of the mixed layer with the sub-mixed layer ocean. The wind induced mixing entrains colder water of the sub-mixed layer ocean into the mixed layer which leads to temperature changes in the SST. This causes increased SST variability in the regions of the trade wind zones as observed and simulated by the fully dynamical ocean models. The seasonal cycle of the mixed layer depth leads to a smaller persistence of the SST variability during the summer, when the mixed layer is very shallow, and to a larger persistence of SST anomalies in winter, when the mixed layer is. This seasonal dependence of the persistence of the SST anomalies can only be simulated by ocean models

that include a seasonal mixed layer parameterization.

The heat exchange of the mixed layer with sub-mixed layer has been simulated in the $MIX_{dynamic}$ model by introducing an ocean heat flux term that damps the SST. This leads to a more realistic SST variability and also decreases the 'redness' of the SST spectra. However, the damping leads to an unrealistic decrease of the SST variance on the decadal time scale. In the simple stochastic climate model, it is assumed that the amount of decadal SST variability is determined only by the integration of the atmospheric heat flux, in which the large heat capacity of the ocean is amplifying the lower-frequency variations. The comparison of the MIX_{50} simulation with the observations and the $MIX_{dynamic}$ simulation leads us to the conclusion that the heat exchange of the mixed layer to the sub-mixed layer ocean is an important process for the SST variability and that the observed increase of the SST variability from the interannual to the decadal time-scale, must be explained by the interaction of the mixed layer with the sub-mixed layer ocean. However, the $MIX_{dynamic}$ simulation fails to simulate this increase at decadal time-scales and it is still not clear whether the characteristics of the decadal SST variability can be simulated by local air-sea interactions at all.

Finally we like to compare the characteristics of the seasonal to interannual SST variability in the midlatitudes with the SST variability of the tropical Pacific. In the tropical Pacific the SST variability is dominated by the El Nino Southern Oscillation (ENSO) phenomenon. It leads to increased predictability in the tropical SST anomalies on the seasonal to interannual time scale, which can only be simulated by fully dynamical ocean-atmosphere coupled models, whereby the horizontal advection and wave propagation in the ocean play important roles. Here we have shown that the SST variability in the midlatitudes is also influenced by dynamical processes in the ocean but, unlike in the tropical Pacific, the spatial and temporal structures of the SST variability in the midlatitudes can be simulated by local air-sea interactions. We have found that the SST variability is strongly influenced by the mixed layer depth variability. We therefore assume that the seasonal and interannual predictability of the midlatitude SST anomalies may be significantly improved by the knowledge of the actual mixed layer depth.

Acknowledgements

We would like to thank Drs. Detlef Mueller and Christian Eckert for fruitful discussions. We thank also Mrs. M. Esch, Dr. E. Roeckner and Mr. U. Schlese for support to implement the mixed layer routine in the ECHAM3 atmosphere model. This work was supported by the European Unions SINTEX project and the German government through its Ocean-CLIVAR and decadal predictability programs

References

- Alexander, M.A., C. Penland, 1996: Variability in a mixed layer ocean model driven by Stochastic atmospheric forcing. *J. Climate*, **9**, 2424-2442.
- Bacher, A., J. M. Oberhuber and E. Roeckner, in press 1998: ENSO dynamics and seasonal cycle in the tropical Pacific as simulated by the ECHAM4/OPYC3 coupled general circulation model, *Climate Dynamics*, in press 1998.
- Bladé, I. 1997: The Influence of Midlatitude Ocean-Atmosphere Coupling on the Low-Frequency Variability of a GCM. Part I: No Tropical SST Forcing. *J. Climate*, **10**, 2087-2106.
- Frankignoul, C., and K. Hasselmann, 1977: Stochastic climate models, II, Application to sea-surface temperature variability and thermocline variability, *Tellus*, **29**, 284-305.
- Frankignoul, C., 1985: Sea Surface Temperature Anomalies, Planetary Waves, and Air-Sea Feedback in the Middle Latitudes. *Rev. of Geophys.*, **23**, 357-390.
- Frey, H., M. Latif and T. Stockdale, 1997: The coupled GCM ECHO-2. part I: The tropical Pacific. *Mon. Wea. Rev.*, **125**, 703-719.
- Hall, A. and S. Manabe, 1997: Can local linear stochastic theory explain sea surface temperature and salinity variability ? *Cilm. Dyna.*, **13**, 167-180.
- Hasselmann, K., 1976: Stochastic climate models. Part I: Theory, *Tellus*, **28**, 473-485.
- Karaca, M. and D. Müller, 1991: Mixed-layer dynamics and buoyancy transports. *Tellus*, **43A**, 350-365.
- Kraus, E. B. and J. Turner 1967: A one-dimensional model of the seasonal thermocline. *Tellus*, **19**, 98-105.
- Latif, M. and T.P. Barnett, 1994: Causes of decadal climate variability over the North Pacific and North America. *Science*, **266**, 634-637.
- Latif, M. , 1998: Dynamics of interdecadal variability in coupled ocean-atmosphere models. *J. Climate*, **11**, 602-624.
- Lemke, P. and T. Manley 1984: The seasonal variation of the mixed-layer and the pycnocline

under polar sea ice. *J. Geo. Res.*, **89**, 6494-6504.

Levitus, S., 1982: Climatological Atlas of the World Ocean, National Oceanic and Atmospheric Administration, 173 pp. and 17 microfiche.

Maier-Reimer, E., U. Mikolajewicz, K. Hasselmann, 1993: Mean Circulation of the Hamburg LSG model and its sensitivity to the thermohaline surface forcing. *J. Phys. Oceanogr.*, **23**, 731-757.

Manabe, S., and R.J. Stouffer, 1996: Low-Frequency Variability of Surface Air Temperature in a 1000-Year Integration of a Coupled Atmosphere-Ocean-Land Surface Model. *J. of Climate*, **9**, 376-393.

Namias, J. and R. M. Born, 1970: Temporal coherence in North Pacific sea surface temperatures. *J. Geophys. Res.*, **75**, 5952-5955.

Namias, J. and R. M. Born, 1974: further studies of temporal coherence in North Pacific sea surface temperatures. *J. Geophys. Res.*, **79**, 797-798.

Parker, D. E., C. K. Folland, A. Bevan, M. N. Ward, M. Jackson and F. Maskell, 1995: Marine surface data for analysis of climate fluctuations on interannual to century time-scales. In: "*Natural Climate Variability on Decadal to Century Time scales*" edited by D. G. Martinson et al. National Academy Press., 241-250.

Roeckner, E., K. Arpe, L. Bengtsson, S. Brinkop, L. Dümenil, M. Esch, E. Kirk, F. Lunkeit, M. Ponater, B. Rockel, R. Sausen, U. Schlese, S. Schubert, M. Windelband, Simulation of the present-day climate with the ECHAM model: Impact of model physics and resolution, Report no.93, October 1992, 171 pp. Available from: Max-Planck-Institut für Meteorologie, Bundesstr.55, 20146 Hamburg, Germany.

Sutton, R.T., M.R. Allen 1997: Decadal predictability of North Atlantic sea surface temperature and climate. *Nature*, **388**, 563-567.

Voss, R., R. Sausen, U. Cubasch, 1998: Periodically synchronously coupled integrations with the atmosphere-ocean general circulation model ECHAM3/LSG. *Climate Dyn.* **14** (4), 249-266.